Structure and durability of opal crystallized glass plates

Léa Brunswic, Frederic Angeli, Laurent Gautron, Thibault Charpentier, Stephane Gin, Pierre Asplanato, Huseyin Kaya, Seong Kim

Structure and durability of opal crystallized glass plates

L. Brunswic[1], F. Angeli[1,*], L. Gautron[2], T. Charpentier[3],
S. Gin [1], P. Asplanato[1], H. Kaya[4], S. H. Kim[4,5]

[1]*CEA, DES, ISEC, DPME, Université de Montpellier, Marcoule, 30207 Bagnols-sur-Cèze Cedex, France*

[2]*Laboratoire Géomatériaux et Environnement (LGE, EA 4508), Université Gustave Eiffel, 5 boulevard Descartes, Champs-sur-Marne, 77454 Marne la Vallée Cedex 2, France*

[3]*Université Paris-Saclay, CEA, CNRS, NIMBE, 91191 Gif-sur-Yvette cedex, France.*

[4]*Department of Materials Science and Engineering, The Pennsylvania State University, University Park, Pennsylvania, USA*

[5]*Department of Chemical Engineering and Materials Research Institute, The Pennsylvania State University, University Park, Pennsylvania, USA*

[*] *Corresponding author: Frédéric Angeli, frederic.angeli@cea.fr*

(Dated: January 6, 2023)

Abstract

The understanding of the ability of glassware products to retain their constitutive elements during alteration in contact with edibles or beverages lies at the core of the REACh topic and food contact regulations. In this study, an opal crystallized glass plate, obtained from the addition of fluorine to a soda-lime base glass has been structurally characterized and altered in food contact like conditions. The investigations on the pristine opal crystallized glass led by optical microscopy, scanning electron microscopy, transmission electron microscopy, X-ray diffraction, ToF-SIMS, solid state NMR spectroscopy and X-Ray Diffraction evidenced the nature of the following crystalline phases: CaF_2, BaF_2 and NaF as well as the distribution of the constitutive elements in the glassy matrix. Overall a continuum of fully vitreous to glass-ceramic material was noticed with different morphology from which we studied two extremes cases: the top surface that resembles a soda-lime glass which was prepared as a slab and the highly crystallized bulk using powder obtained from the grinding of a plate. Powder and slab were altered together at 70 °C in acetic acid 4 % (v/v) imposing a pH of 2.4 in an airtight container for 231 days to 3 years. Kinetics of alteration were determined through ICP-AES analysis of regular alteration medium samplings. Although originating from a single item, the powder and slab did not show the same behaviour. The bulk powder alteration is characterized by a predominant hydrolysis phenomenon impacting the crystals and the glassy matrix at the same rate, leaving no remaining altered layer at the surface whereas a 1.25 ± 0.022 µm thick alteration layer was observed by Spectroscopic Ellipsometry on the smooth surface of the plate after 231 days. The mechanisms for the formation of this altered layer as well as the differences between the powder, representative of the bulk opal crystallized glass and the slab that remains the actual surface in contact with edibles are discussed in the article.

INTRODUCTION

Opal crystallized glass is a choc resistant, heat resistant and endlessly tailored material widely used for tableware and cookware. This unique material brings together two opposite features of material sciences: an amorphous matrix, that can be qualified as glass, and well-ordered crystals embedded in the matrix, making it a glass-ceramic. Three different crystalline phases originating from the addition of fluorine to a soda-lime base composition are bringing color and opaqueness to this material. Opal glass items are used repeatedly on a daily basis to hold in edible contents requiring sturdy and lasting durable properties, especially regarding food contact. The International Standards Organization has established acetic acid 4 % (v/v) as food substitute for testing standards shedding the light on the lack of scientific knowledge on glassy matrices' chemical durability under acidic conditions and specifically glass-ceramics Stone-Weiss et al. (2020). A plate made of opal crystallized glass has been studied in light of silicate glass alteration to improve the understanding of the migration of elements between the glass-ceramic and the food substitute over years. Based on standardized test ISO 7086 Ceramic cookware in contact with food — Release of lead and cadmium — the alteration of bulk powder and a slab representative of the actual surface of the plate were altered at 70 °C in acetic acid 4 % (v/v) for three years and monitored through characterizations of the surface and the alteration solution.

All opal plates start with a gob of fused glass dropped at the center of a steal mould and immediately centrifuged to reach the desired size and thickness of glass. From a macroscopic point of view it forms a white plate, almost opaque, with two large and almost flat surfaces: the top and the bottom. Optical microscope images of both sides and the width of the plate are presented in figure 1. The bottom side of the plate lies in contact with the steal mould during the shaping process, resulting in two major differences between the top and the bottom sides: *i)* the bottom side exhibits a microscopic roughness visible in figure 1b , which is not the case of the top face that remains smooth (figure 1a) *ii)* the cooling rates of the two sides are different as the top side is only in contact with the atmosphere which has a poor calorific capacity, especially compared to the steal mould, strongly impacting the crystallization process in the glass. This process results in plates with two non equivalent faces and macroscopic heterogeneous distribution of the crystalline phases width-wise. The glass structure before alteration is described for purposes of comparison with the after alteration case but not discussed as too many industrial parameters that cannot all be divulged come into play. To embrace the diversity found in a sample plate this material was

studied under two different forms: powder, corresponding to the average bulk, dominated by a glass-ceramic structure, and a slab cut from a plate and representative of the real case surface in contact with edibles. The composition of the bulk powder was determined by complete acidic dissolution and is given in table I.

oxide	SiO_2	Na_2O	Al_2O_3	CaO	BaO	K_2O	F_2
mol%	73.6	11.9	4.8	2.2	0.8	1.0	5.7

TABLE I: Bulk glass composition in molar percent of oxide analyzed by ICP-AES after complete acidic dissolution. The relative uncertainty on these measurements is considered to be 20 %.

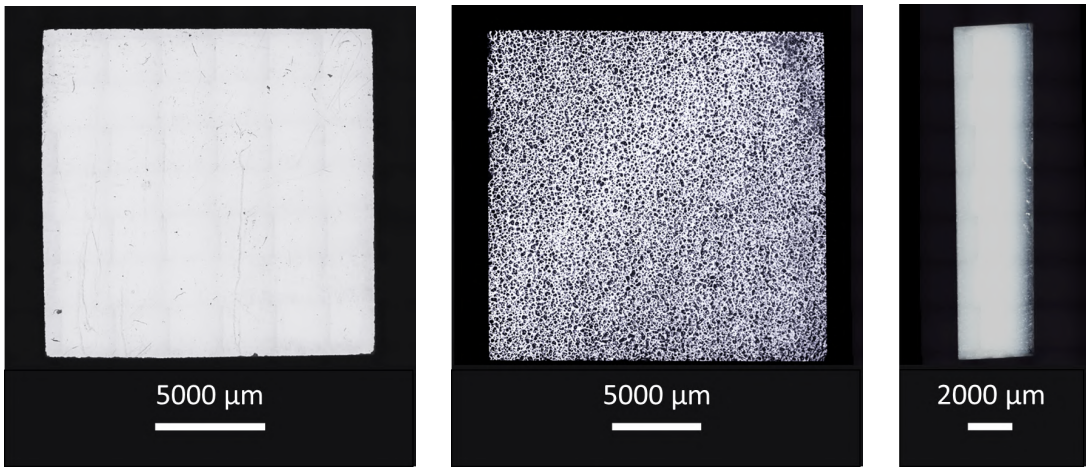

(a) top face (b) bottom face (c) plate's width

FIG. 1: Optical micrographs of an opal crystallized glass slab cut from the middle of a plate with 1a the top face of the plate with a smooth aspect, 1b the bottom face which exhibits important roughness and 1c a view of the total width of the plate with the smooth top side along the left long side and the rough bottom side along the right long side.

I. RESULTS AND DISCUSSION

A. Pristine glass structure

a. SEM The observation of a cross-section comprising the entire breadth, 4 mm, of a plate including the top and bottom faces showed different degrees of heterogeneity in terms of phases and distribution of theses phases although the distribution of silicon, the main glass constituent, seemed homogeneous throughout the sample. Crystals are embedded in a glassy matrix with different glass/crystals ratios depending on the distance to the top. The first observable crystals under these conditions were located 9 µm below the top surface, and their measured diameter was about 60 nm. 20 µm below the surface the average diameter of the crystals measured was increasing to 90 nm, in correlation with the mapping of fluorine, given in figure 2, which appears completely depleted from the first 7 µm area and then gradually increasing as the crystal's diameter grows. The larger crystals were found in the center region spreading across the majority of the sample's breadth and measured up to 200 nm with an homogeneous distribution within the glassy matrix. No crystals were observed in the 100 µm closest to the bottom surface although the chemical mapping clearly shows the presence of F except for the last 3 µm. As a matter of fact, crystals with a diameter inferior to 50 nm could not be detected through this technique but the probability of these nanocrystals was answered later on thanks to solid state NMR spectroscopy data. Sodium also showed a very peculiar gradient of distribution near the top surface with the outermost 4 µm exhibiting a strong presence of Na followed by a depleted region shifting through a smooth gradient to the base level of sodium found throughout the majority of the sample. The same pattern was observed from the bottom face spreading on a twice smaller area.

b. Tof-SIMS In accordance with SEM, Tof-SIMS showed for the smooth face analysis, a top 4 µm thick layer enriched in Na, Ba and Ca as observed in figure 3a. Moreover Si, Al and K appeared depleted from the top 6 µm of the sample, which could be foreseen from the top air side chemical mapping of Si in figure 2 but did not clearly show for Al and K. Since the Tof-SIMS profile could not be made quantitative as the ion yields depend both on the element and the local matrix, and no internal standard element could be used, great variations of intensity don't necessarily account for great concentration changes in the glass. But Tof-SIMS sheds light more precisely on the first hundreds of nanometers that could not be observed via SE microscopy and displayed a very peculiar distribution of elements among the first 200 nm completely different from

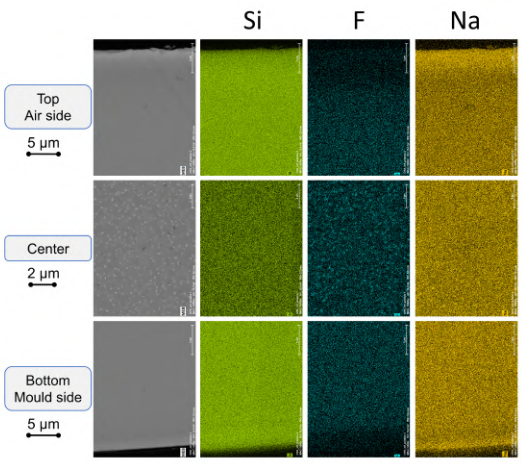

FIG. 2: SEM micrographs (backscattered electrons) of the top, middle and bottom regions of a cross-section from an opal crystallized glass plate and EDS mapping of Si, F and Na from the same regions.

the previous observations. Figure 3b presents a similar trend for all elements analyzed except Na: steeply decreasing gradients until 180 nm depth followed by a stabilization of the signals slowly starting to show the trends confirmed by the deeper analysis on the left hand side. On the opposite, Na was quite depleted from the top 180 nm before entering the enriched area observed between 0 and 4 µm in figure 3a. Given that the first 180 nm layer was also hydrated as seen on Tof-SIMS profiles of H, SiOH and Na (available in the figure S14 of the supplementary information), the depletion of Na could be seen as the result of first stage atmospheric alteration due to the storage of the glass Chopinet et al. (2008), Majérus et al. (2020) between its production and the start of the experiment. A greasy deposit composed of sodium carbonates typically occurs at the surface of the glass after 4 weeks of storage at room temperature and humidity. No crystals of sodium carbonate were observed in our case but they might have been eliminated by washing beforehand as the storage duration exceeded 4 weeks. An analysis of the bottom face has been conducted but could not be validated because of the surface roughness, as shown in figure 1b.

c. NMR spectroscopy The powder obtained from the crushing, grinding and sieving of a commercial plate was analyzed by Magic-Angle Spinning (MAS) NMR spectroscopy giving an overview of the average predominating structure of opal crystallized glass plates. The optical properties of the same opal crystallized glass were studied by Rio et al. Rio et al. (2021) and it was determined that crystals represented 8 wt% of the material, otherwise constituted of 92 wt% of glassy matrix. The fluorine-19 MAS NMR spectra collected from pristine opal crystallized glass

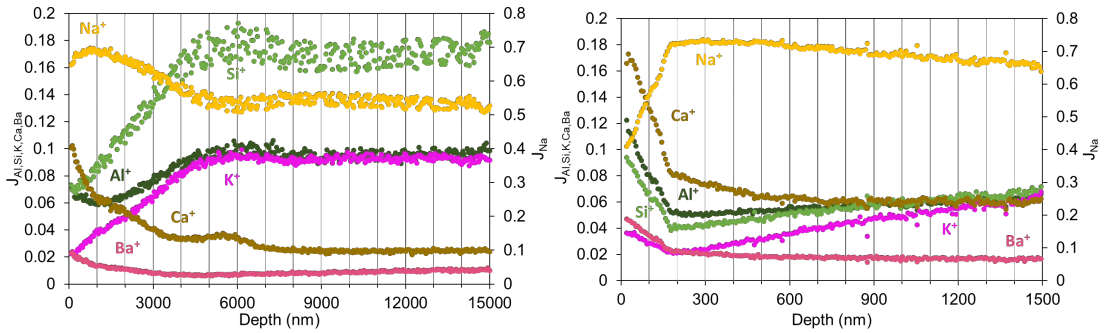

(a) ToF-SIMS profiles until 15 µm

(b) ToF-SIMS profiles until 1.5 µm

FIG. 3: Tof-SIMS profiles obtained from the analysis of the smooth face of a pristine opal crystallized glass plate. The ions displayed represent the species detected by the mass spectrometer after sputtering. The signals are normalized to the total intensity. Signals from Al, Si, Ca, Ba and K are read on the left hand Y-axis and signal from Na is read on the right hand Y-axis.

powder, represented in figure 4a, show the presence of 3 crystallized compounds: NaF, CaF_2 and BaF_2, and a glassy amorphous matrix. This technique allows the quantification of these phases by fitting the peaks yielding a distribution of Na and F among the different phases that has been reported in figure 4b and 4a respectively. 11 % of the total fluorine molar content was found in the glassy matrix, as shown in the zoomed spectra with purple dashes, explaining the bottom region with chemical mapping of F but no crystals in figure 2 as part of fluorine is dissolved in the glassy matrix. The highest contribution of F goes for the NaF crystallized phase with 64 % of F consumed far from the 22 % for CaF_2 and 2 % for BaF_2 crystals. 1 % of the total area of the spectra occurred as a line at -98 ppm and was assigned as an unknown phase (uP). It is most probably a very little fraction of CaF_2 forming a solid solution with another cation or a lone phase arising from the presence of very small amounts of impurities in the glass forming its own phase. Considering the ^{23}Na spectrum (figure 4b), the fitting yields 34 % for the glassy matrix and 66 % for NaF contribution, accounting for all the transitions detected, namely central and satellite, of the Na sites from NaF and only the central transitions from the Na sites in the glassy matrix. Hence the normalization of the contribution from the NaF crystals to the intensity of the central transition only for the appropriate ℓ and m values Freude and Haase (2019) giving a final output of 43.8 % for the NaF crystallized phase and 56.2 % of Na located in the glassy matrix. In summary, the high sensibility of ^{19}F nucleus provided fine information on fluorine and earth-alkali elements

distribution: most of the calcium content is crystallized, 81 % of Ca is incorporated under the form of CaF_2, as opposed to barium with only 20 % found in the crystalline phase. Although fluorine remained the main constituent of the crystallized phase, part of fluorine is dissolved in the glassy matrix. Data regarding sodium emerged from the cross-checking of ^{19}F and ^{23}Na MAS NMR fits, both data sets agreeing on 43 % of the total sodium found in the NaF crystals and 57 % Na in the matrix lowering the Na_2O content of the glassy matrix to 6.7 mol%. Aluminum in this material has also been investigated with ^{27}Al MAS NMR demonstrating the presence of Al in the glassy matrix only and almost exclusively under tetrahedral configuration (figure S15 in supplementary information). A very small contribution of 6-fold coordinated Al atoms was noticed and estimated to be inferior to 1 % with no impact on the global structure.

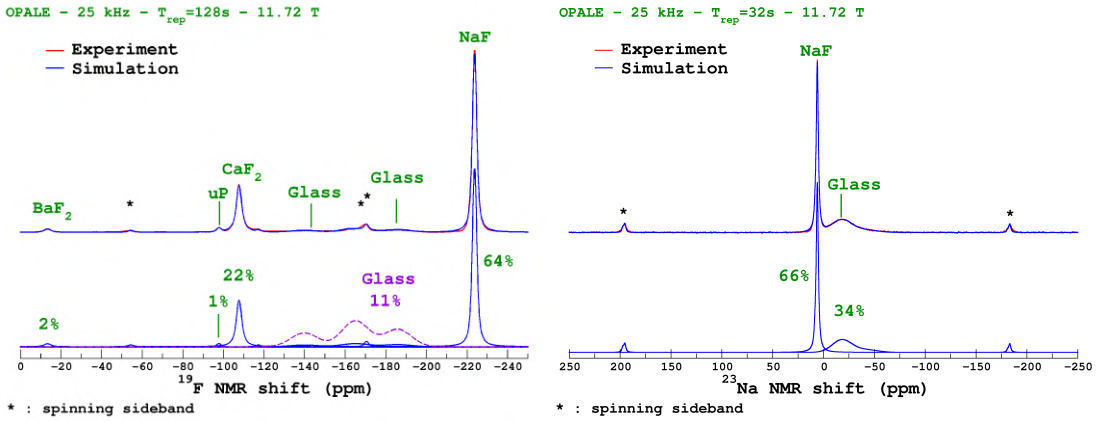

(a) ^{19}F MAS NMR

(b) ^{23}Na MAS NMR

FIG. 4: Experimental and simulated MAS NMR ^{19}F (4a) and ^{23}Na (4b) obtained from pristine opal glass powder at 25 kHz and 11.72 T. The glass contribution in figure 4a (purple dashes) is zoomed.

d. X-Ray Diffraction The pristine opal glass was also characterized by X-Ray Diffraction: the XRD pattern is presented in the figure 5. It is typical of a glass embedding crystals like in a glass-ceramic, with large "bumps" characteristic of the vitreous matrix, from which we see Bragg peaks related to the different crystals. The three expected crystals were identified: NaF, CaF_2 and BaF_2, from the crystal structures of villiaumite (halite-type), fluorite and frankdicksonite (fluorite-type) respectively, as referenced on the website MinCryst (http://database.iem.ac.ru/mincryst/).

e. Transmission Electron Microscopy TEM was used in order to try to answer some questions as asked above, in particular on the presence of crystals on a nanometric scale and on the variations

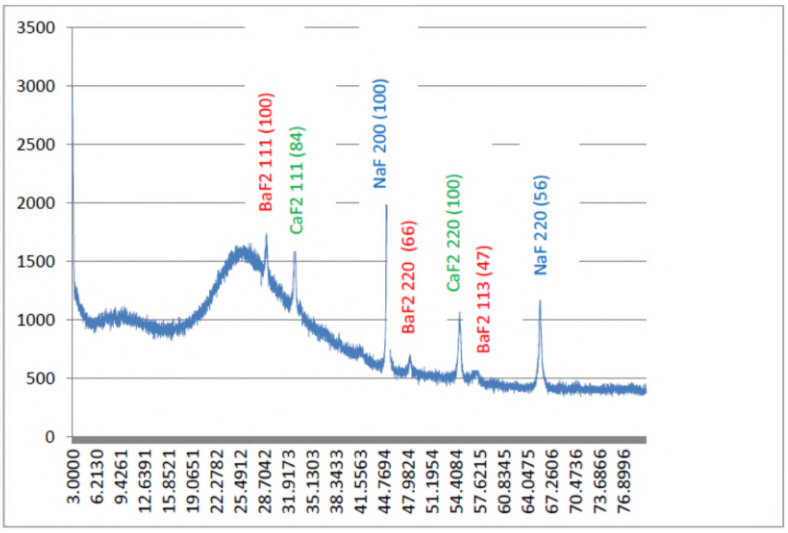

FIG. 5: X-Ray Diffraction pattern obtained from the pristine opal glass powder.

in composition over distances of the order of a few hundred nanometers. First, we could observe and identify the different crystals embedded in the glass matrix, as shown in the figure 6. The specific size of each crystal was observed as follows: NaF in range 150-200 nm, CaF_2 in range 50-100 nm and BaF_2 in a range 20-30 nm. In the figure S16 (in the supplementary information), we present a typical TEM image of a selected area from the pristine opal glass slab (the top air smooth surface is at the bottom of the image), with EDS mappings of Na and F from the same region: we could observe large crystals of NaF, relatively close to the surface (about 500 nm). Note that this selected size-limited area is probably not representative of the sample, since usually we did not observe crystals under the smooth surface in a zone of approximately the same thickness as that observed by SEM (about 9 µm). As evidenced in the figure 3 from the ToF-SIMS analysis, the profiles revealed some clear trends for Na, K, Al, Ca and Ba, both on large and small scales (15 µm vs 1.5 µm). In order to confirm these trends, we performed composition profiles using TEM-EDS. Figure 7 gives the profiles for Na, Ba and Ca (7a) and for Si and Al (7b). As for ToF-SIMS, we observed a layer enriched in Na, Ba and Ca under the smooth surface of the sample, but the decrease of the concentration was not the same for these elements: the layer was about 4 microns thick for sodium, 3 microns for calcium and 1 micron for barium. We observed a peak of sodium near the surface: it can be expected that the application of a double protective layer of palladium and platinum can favor the movement towards the surface of certain elements, which seemed to be the case in particular for sodium. Note that the elemental distribution among the first 200 nm did

not show clear trends similar to those observed in ToF-SIMS. Finally, contrary to the ToF-SIMS results, the profile for Si revealed a small depleted zone at the extreme surface (about 200 nm) then an enrichment followed by a slow decrease down to about 4.5 µm.

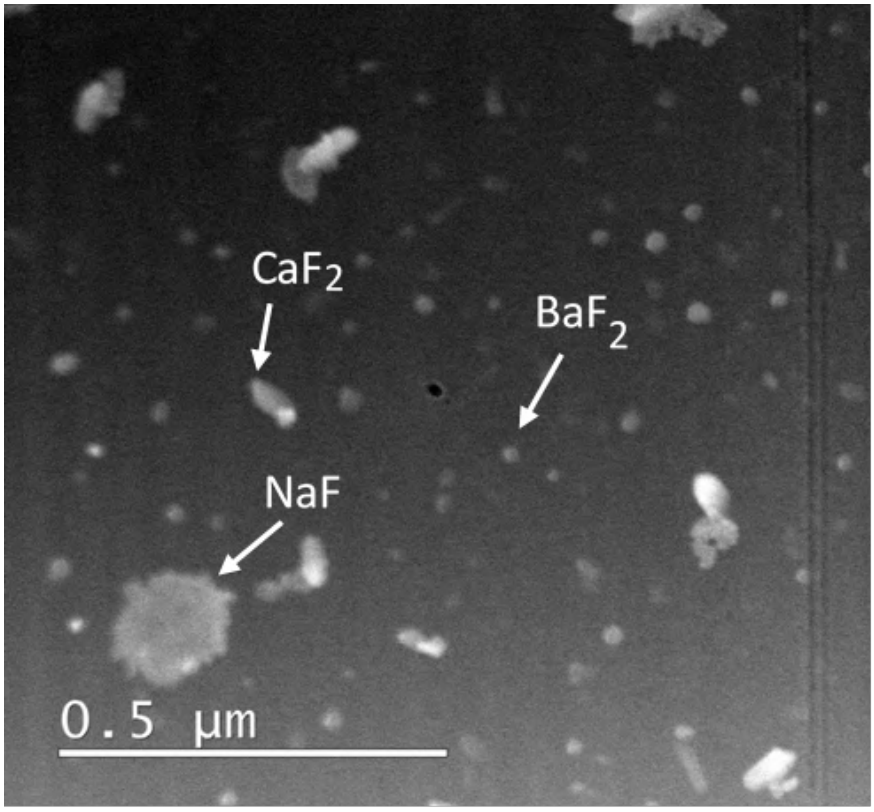

FIG. 6: TEM image of a selected area of the pristine opal glass slab.

B. Chemical durability in acidic medium

a. bulk - leaching rate As the alteration reactor contained both powder and monolith, it was estimated through surface measurements that the glass powder was responsible for 97 % of the glass surface exposed to the acidic solution, thus it can be considered that the elements leaching out of the glass from which the kinetics were calculated, account for the alteration of the bulk glass rather than the slab's surfaces. Consequently, the calculations based on the sampled solutions are representative of the alteration of the glassy matrix and the crystals embedded in it indiscriminately, as these two components cannot be deconvoluted easily. The resulting alteration can be described as an initial release of elements in solution followed by a leaching behaviour linear with time as seen in figure 8. As expected, the most released element was

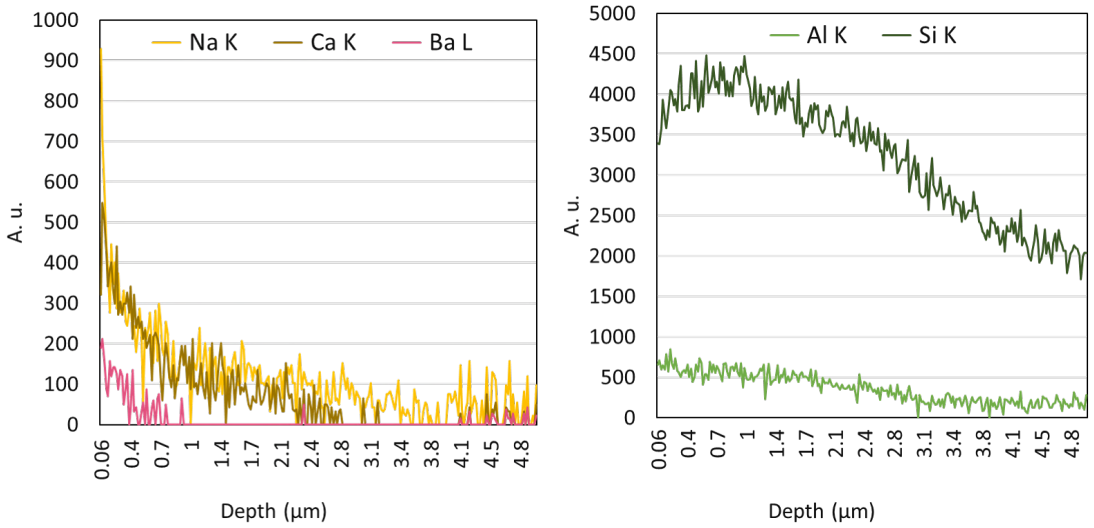

(a) Na, Ca, Ba TEM-EDS

(b) Si, Al TEM-EDS

FIG. 7: EDS profiles obtained from the analysis of the smooth surface of a pristine opal crystallized glass plate under TEM. The vertical axis scale is given in arbitrary units.

sodium with a diffusion coefficient calculated from equation 5 $D_{Na} = 6.1\times10^{-21}m^2.s^{-1}$ after 28 days of alteration. After a month of alteration, the equivalent thickness of sodium stopped being clearly linear with the square root of time but showed a direct linear dependency towards time meaning that the rate of hydrolysis was very close to the rate of interdiffusion. Overall the predominant leaching mechanism remained the hydrolysis of the glassy network for every glass constituents after 28 days. No trend variation was observed all along the three years during which the experiment was carried out and the hydrolysis rate was calculated from equation 4 yielding $r_{Si}(t) = 2.6\times10^{-3}$ $g.m^{-2}.d^{-1}$. The markers of Ca have intentionally been made unobtrusive in figure 8 as this element was very much subjected to lab contamination resulting in noisy analytical data and unusable rate calculations. But the behaviour of calcium is expected to closely resemble the one of barium as observed from the Tof-SIMS data acquired after 231 days of alteration shown in figure 10.

b. bulk - remaining alteration layer After 1096 days (3 years) of alteration, the ETh values calculated from equations 1, 2 and 3 for network-forming elements Si and Al were the lowest,as expected from the structure, with $ETh_{geo} = 1.20\pm0.04$ µm, quickly followed by ETh of Ba and K and capped by Na with $ETh_{geo} = 1.87\pm0.06$ µm. The values were calculated considering a geometrical approximation of the glass powder's surface as explained in subsection II C and

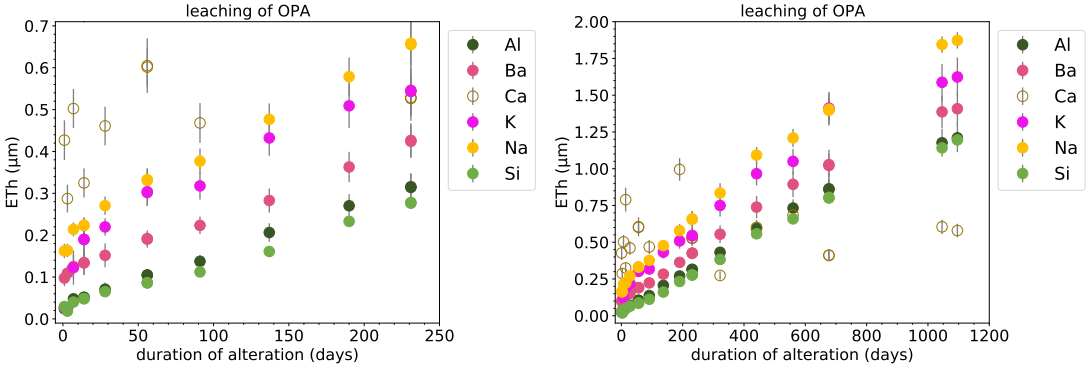

(a) leaching until 250 days

(b) leaching until 3 years

FIG. 8: Equivalent Thickness (ETh) calculations from ICP-AES data and geometric approximation of the glass surface of the main elements through time for opal glass powder at 70 °C, pH = 2.4.

equation 1. To figure out the impact of the surface measurement hypothesis on the calculated ETh values, the glass surface was also measured by BET method supplying a surfaces' ratio S_{BET}/S_{geo} of 1.83, which is slightly lower than the 2.5 ± 0.2 value typically given as a reference and showed a closest agreement between geometrical and BET methods than usually found in the literature Fournier et al. (2016). From the final picture given by ETh calculations presented in figure 8, a remaining alteration layer depleted in sodium of 0.67 ± 0.1 µm according to the geometrical approximation of the glass surface and 0.37 ± 0.05 µm from the BET measurements should be observed. The remaining alteration layer was estimated by subtracting the ETh of Si, which represents the fully dissolved glass, to the ETh of Na, the most leached out element. To try to discriminate between these two methods the glass powder altered for 3 years (1096 days) was prepared as a polished cross section and observed by SEM. Figure 9 shows a global view of a glass particle after alteration with homogeneous distribution of Na and Si across the sample. On the closer view of the particle's edge no remaining alteration layer depleted in sodium was observed. The sensitivity of the SEM observations under these conditions is estimated to differentiate accurately highly depleted layers in sodium of 0.5 µm width and above. The absence of sodium depleted layer observed could be due to a width too thin to be imaged via this microscopic scanning method or to the partial depletion of the altered layer leading to insufficient contrast detected by SEM-EDS of Na between the pristine and altered zone and potentially both hypothesis combined. Overall, hydrolysis resulted as the main alteration mechanism of the bulk

powder with close leaching kinetics for all the glass constituents measured in solution and no characterized sign of interdiffusion remaining on the powder after 3 years of alteration observed by SEM-EDS microscopy.

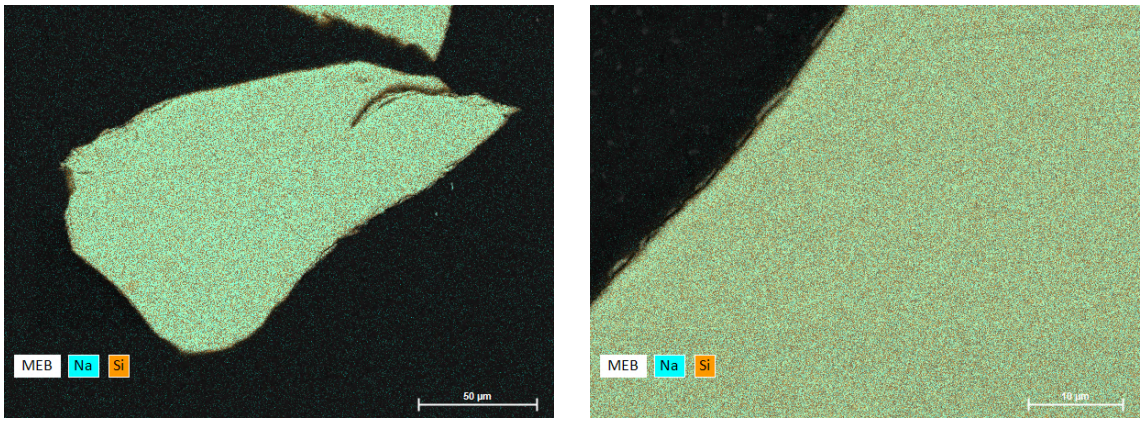

(a) x500 (b) x2000

FIG. 9: SEM micrographs (backscattered electrons) and EDS mapping of Si and Na of a grain of glass after 3 years of alteration at 70 °C, pH = 2.4 prepared as a polished cross section.

c. slab - remaining alteration layer According to SEM mapping and ToF-SIMS profiles conducted before alteration on identical samples (figure 2 and 3), the top first 5 µm of the smooth face did not contain fluorine nor crystals detectable through SEM (diameters superior to 50 nm), in other words the glass discussed hereafter had a vitreous aspect with sodalime-like composition. After 231 days of alteration the glass slab was removed from the reactor. Surface characterizations were then conducted on the smooth face of the altered slab showing a total alteration depth of 1.40 µm estimated thanks to the ToF-SIMS profiles of H^+ and $SiOH^+$ as displayed in figure 10b and 1.25 ± 0.022 µm according to the measurement conducted by spectroscopic ellipsometry presented in figure 11. During ellipsometry data processing, an optical model that represents the sample surface is built with initial guesses for alteration layer thickness and porosity. Theoretical Ψ and Δ which would be generated upon reflection from this optical model are calculated. The difference between experimentally measured Ψ and Δ from the sample and theoretical Ψ and Δ that are calculated with the model is minimized by fitting the fitting parameters (alteration layer thickness, porosity). In the plots in figure 11, model curves are the theoretical Ψ and Δ calculated with the "optimized" model obtained with fitted parameters. ToF-SIMS and Spectroscopic Ellipsometry are in good agreement although their probing area are very

different. ToF-SIMS was carried out on a 50 x 50 µm² zone whereas spectroscopic ellipsometry was ran on a ≈0.5 cm² area, probing a much larger area and yielding a very reliable average value of the global alteration of the smooth slab's face. The remaining alteration layer is mainly depleted in sodium, absent throughout most of its depth which can only be explained by a dominant ion-exchange/interdiffusion mechanism of alteration regarding sodium, as typically observed in silicate glasses alteration Bunker (1994), Sinton and LaCourse (2001). The very weak depths depleted in Al, Ca and Ba are better shown in the detailed plot shown in figure 10a. A highly similar behaviour was observed for earth-alkali Ca and Ba, both exhibiting a 47 nm depleted area at the surface followed by a swift increase and then a slowly decreasing plateau. This plateau could correspond to the initial level of Ca and Ba present in this region of the glass, although the normalized intensity remained above 1, because the profiles collected before alteration (figure 3) clearly showed a continual decrease of Ca and Ba signals in the first 5 µm of the pristine glass. As a matter of fact the profiles displayed in figure 10 were normalized to a single value averaged from the non hydrated segment of the sample analyzed, which explains the apparent enriched area in Ca and Ba both as an artefact from the normalization and the heterogeneity of distribution depth-wise of these elements prior to alteration. Although very consistent in their behaviour throughout ToF-SIMS and SEM observations so far, Si and Al exhibit different distributions in the outermost 20 nm of the 231 days-altered glass surface which appeared depleted in Al leaving behind an Si-rich and highly hydrated surface layer. The profile obtained for potassium showed a small area about 100 nm width near the surface fully depleted in K and followed by a bump spreading across 1.1 µm with normalized intensities above 1 before decreasing to a stable level of intensity corresponding to non-hydrated and thus non-altered glass. The same variations were noticed through TEM-EDS analysis as shown in figure 10d) excluding a simple matrix effect artefact from the ToF-SIMS profile. The peak near the extreme surface (0-0.3 µm) is probably due to the presence of the Pt-Pd protection layers deposition which could promote the migration of elements like K. The enriched area in potassium between positions 0.5 and 1.8 µm was also observed by ToF-SIMS and could compensate the depletion of sodium in this same area. In figure 10 a plot featuring the profiles of Na and K only is given and the severely sodium depleted zones appeared to be the locations where potassium is retained. The opposite reciprocity of the distribution of these elements in the remaining altered layer let us think that potassium played a role in compensating the absence of sodium during the alteration process and raises the question of the origin of the potassium locally accumulated in the alteration layer. The origin of potassium can be twofold: *i)* from the glass,

through the internal migration of potassium contained in the underlying pristine glassy matrix towards the solution through the alteration layer fostered by exchanges with solution's protons that have penetrated in the glass, *ii)* potassium from the container or the solution, unwillingly present, often brought by pH electrode or other kinds of contamination resulting in external additions of K to the alteration medium. In the glass alteration literature, external additions of KCl salt to the alteration solution are reported to study the alteration kinetics decrease caused by the incorporation of cations (K, Cs, Li, Ca) in the alteration layer Aréna et al. (2019), Collin et al. (2018). In these studies the weakest concentrations of potassium studied to obtain a sensitive effect are at least a hundred times greater than the concentration reported here. Indeed after 231 days of alteration, the solution was far from saturation regarding potassium or sodium as claimed in figure 8 by the absence of plateau. Thus, it is likely that the potassium observed in the alteration layer in figure 10 is of endogenous origin, that is not diffusing from the alteration solution into the glass sample under alteration but from the internal layers of the glass towards the external layers. Finally, the ToF-SIMS profiles highlight a 100 nm width zone between 1.3 and 1.4 µm's depth with the presence of protons and sodium, significant of the higher diffusion coefficient of protons into the glass than the diffusion coefficient of Na out of the glass.

TEM-EDS analysis of the opal altered glass As evidenced by TEM, we observed no crystal in the surface layer about 5 to 6 µm thick, as shown in figure 7. In-depth monitoring of the sodium content seemed to be a good indicator for the identification of the alteration layer. We observed a depletion of Na in a region about 1.5 µm thick below the smooth surface of the altered opal glass, as shown in figure 12a. This result is consistent with those from ToF-SIMS and spectroscopic ellipsometry, which proposed an alteration layer thickness ranging from 1.25 to 1.40 µm. The Na content profile is presented in figure 12b: it displayed a depleted zone about 1.5 µm thick below the surface, then an enrichment in sodium, which content then decreased slowly to a depth of about 5 microns as already observed on the pristine glass by ToF-SIMS (figure 3a). It is assumed that the alteration layer corresponds to this layer 1.5 µm thick depleted in Na.

We also realized EDS-TEM profiles for the other elements, to compare them to those obtained by ToF-SIMS and presented in the figure 10. For Ca and Ba, we got almost the same results (see figures S17a and S17b respectively in the supplementary information): for Ca the profile is the same, with a narrow depletion layer (about 50 nm thick) at the extreme surface, then a swift increase followed deeper by a slowly decreasing plateau. For Ba, the extreme surface

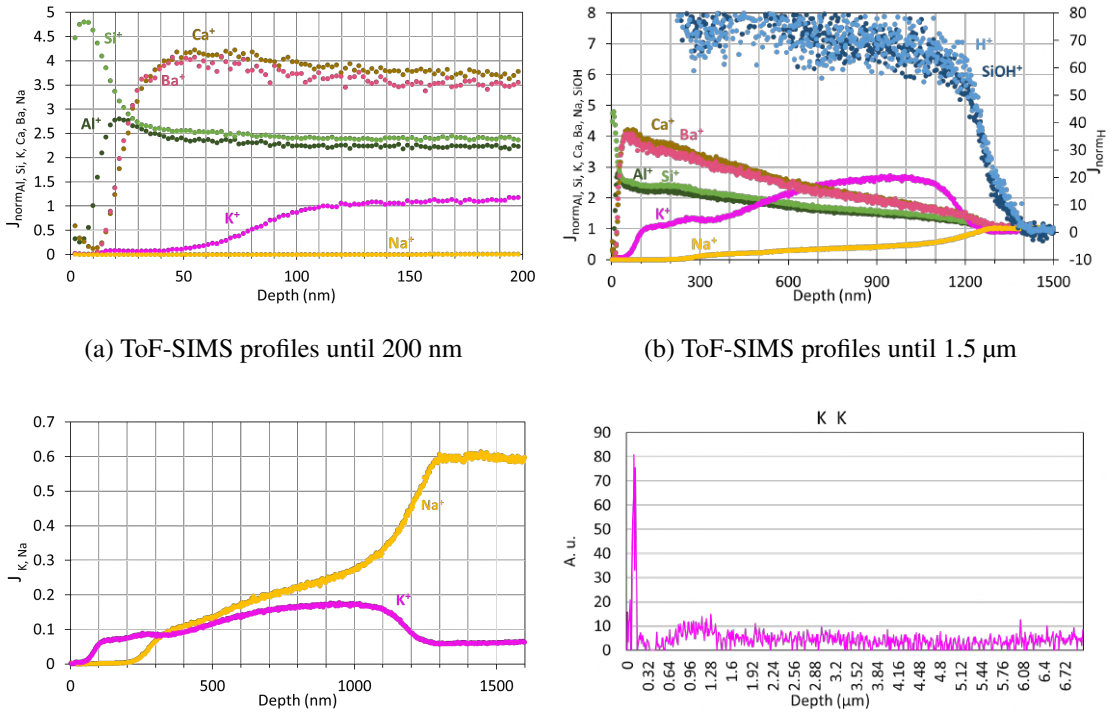

(a) ToF-SIMS profiles until 200 nm

(b) ToF-SIMS profiles until 1.5 µm

(c) ToF-SIMS profiles of Na and K until 1.5 µm

(d) TEM-EDS K

FIG. 10: 10a, 10b, 10c: Tof-SIMS profiles obtained from the analysis of the smooth face of a slab from an opal crystallized glass plate after 231 days of alteration at 70 °C and pH = 2.4. The ions displayed represent the species detected by the mass spectrometer after sputtering. The signals are normalized to the total intensity and to the pristine glass for the plots 10a and 10b. 10d: TEM-EDS profile of K (K-spectral line) obtained from opal glass plate slab smooth surface altered 231 days at 70 °C in acetic acid 4 %vol (pH = 2.4).

depleted layer is not clearly evidenced but the following zones are present. For Si and Al, we obtained roughly the same results as those presented for ToF-SIMS (figure 10a): the narrow region where Al and Si exhibit different behaviour is probably more about 40 nm thick just below the extreme surface (see figure S18, in the supplementary information). The swift increases of both concentrations are actually shifted, with the Si profile increasing about 20 nm before that of Al, and both profiles reached their maximum point over a region of about 40 nm thick.

d. slab - leaching rate In the same reactor opal crystallized glass plates was altered under two different forms: powder and slab. The remaining alteration layer have been carefully characterized in both cases but only the kinetics of the powder is available. Applying the kinetics obtained on the powder to try to match the final picture given by characterizations of the slab after

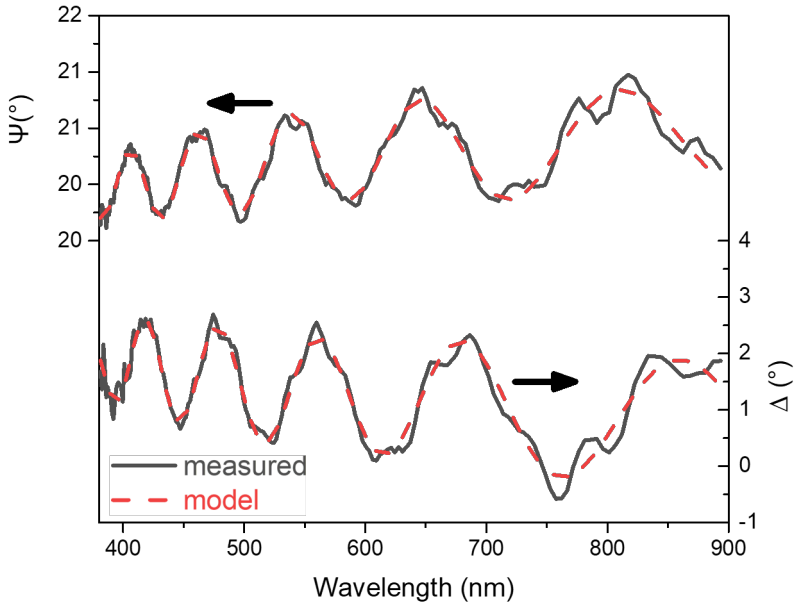

FIG. 11: Experimental ellipsometric spectra (in Ψ and Δ) of opal crystallized glass plate altered 231 days at 70 °C and pH = 2.4, measured at room relative humidity. The dashed lines are fittings to experimental data.

231 days of alteration is possible by taking into account the shape factor described by Fournier et al. in Fournier et al. (2016). Theoretically the ratio of alteration rates obtained on powder (with geometrical approximation of the surface) versus slab is $F_s = \frac{R_{0_{powder}}}{R_{0_{slab}}} = 1.3 \pm 0.3$ which can also be expressed as $F_s = \frac{ETh_{X_{powder}} - ETh_{Si_{powder}}}{ETh_{X_{slab}}} = 1.3 \pm 0.3$ with X a glass constituting element measured in solution and $ETh_{X_{slab}}$ the depth depleted in element X from the ToF-SIMS corresponding profile. The shape factor obtained for the elements depleted after 231 days are given in table II. The calculated F_s values do not range into the limits determined by Fournier et al. displaying great discrepancies between the powder and slab alteration rates that cannot be only imputed to the shape of the glass. Other conceivable reasons for such differences between glass powder and slab are multiple and intertwined. Firstly the structures of both preparations were different. The glass slab exhibited a vitreous outer layer and no crystals in the area that has been affected by alteration until 231 days. Oppositely the glass powder is predominantly composed of grains with a high density of 50 to 200 nm crystals embedded in a crystal matrix. Secondly the composition are not strictly equivalent. In the case of glass powder

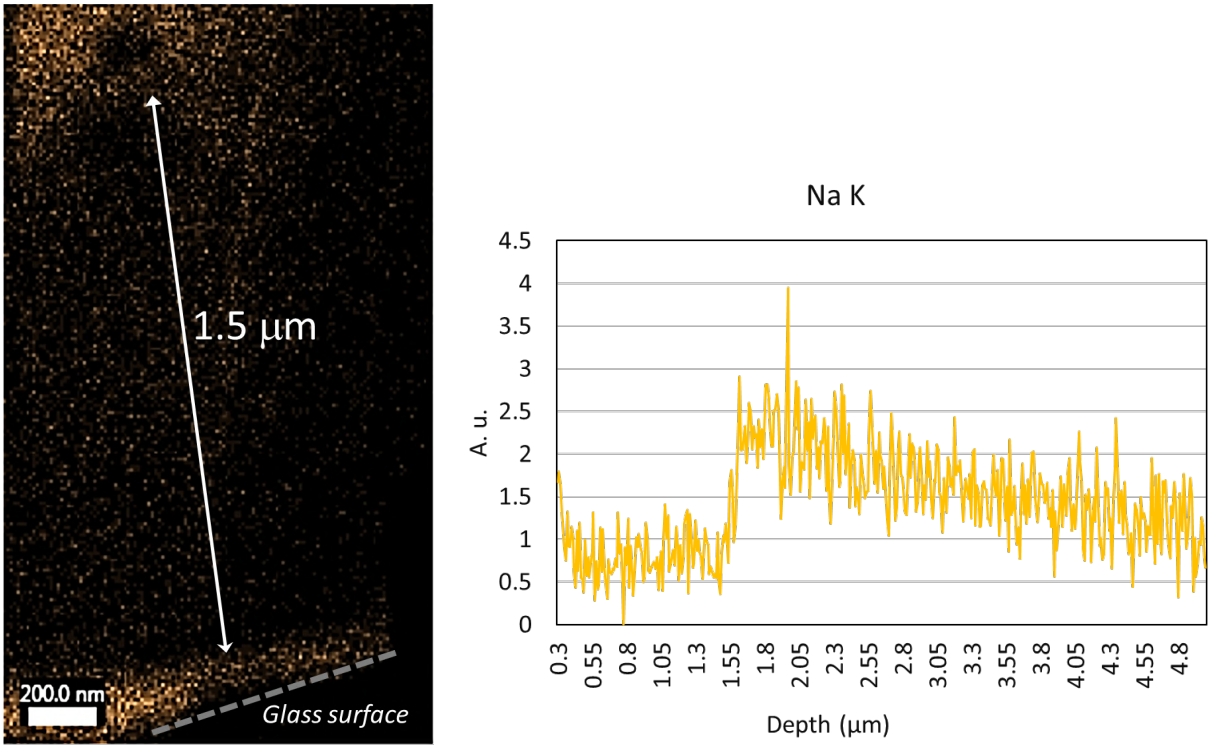

(a) Na mapping

(b) Na profile

FIG. 12: 12a EDS mapping of Na in a selected area of the 231-days-altered opal glass. The surface of the altered glass slab is indicated by the dotted line at the bottom of the picture. 12b EDS profile of Na from the smooth surface of the altered opal glass. The horizontal axis scale is in microns.

there is a structural heterogeneity as discussed there-before resulting in 2 very different but closely interwoven phases, which global composition is constant at a grain scale. But the composition of the glassy matrix only could not be measured as the great magnification required to hit in between crystals caused the well known migration of alkali from the glassy matrix under the electron beam, altering the targeted composition. Regarding the slab the situation is opposite with a structurally homogeneous material but undeniable variations in elemental distribution as shown in figure 2. Therefore besides the presence of crystals in the powder, it is also hard to appreciate and quantify greater concentrations of alkali at the surface of the slab that would obviously affect the alteration mechanisms of the object. Consequently, the chemical durability of the surface of the plate cannot be considered as equivalent to the one of the bulk in terms of rates as well as mechanisms of alteration. As a matter of fact, the slab's alteration is dominated by interdiffusion after 231 days in acetic acid 4 % (v/v) at 70 °C when the kinetics given by the powder show the preponderating

role of hydrolysis under the very same conditions.

element	F_s
Na	0.27
K	0.21
Al	1.89
Ba	3.16
Ca	5.34

TABLE II: Shape factor calculated from solution analysis and ToF-SIMS profiles for Na, Al, Ba, Ca and K in opal crystallized glass plate after 231 days of alteration at 70 °C and pH = 2.4.

e. Structure of the altered bulk glass After 969 days of alteration, powder was sampled from the reactor and analyzed by NMR spectroscopy again to investigate structural changes of sodium and fluorine caused by the long term bathing in acetic acid 4 % (v/v) at 70 °C. The spectra collected after alteration for ^{19}F and ^{23}Na nuclei are presented in figure 13. All the ^{19}F spectra given in figure 13a and 13b were acquired with 256 seconds recycling delay to allow full comparison of the data on pristine and altered glass including quantification. As shown by the overlap of the spectra, the results obtained are fairly the same before and after alteration, validating a congruent dissolution mechanism of glass and crystals simultaneously. Regarding sodium, the quantification of the crystalline phases from the ^{23}Na MAS NMR spectrum after alteration (figure 13c) yielded 43.5 % of Na distributed in the NaF crystals and 56.5% in the glassy matrix which remained very close to the proportions calculated before alteration (43.8% and 56.2% respectively). Nonetheless, a slight decrease of the width of NaF line after alteration can be noticed regarding this compound probed by ^{23}Na and ^{19}F MAS NMR (figures 13c and 13a respectively). This feature indicates the mild reduction of the quadrupolar coupling constant which is characteristic of the hydration and thus the alteration of glass Engelhardt and Michel (1987). This observation is well correlated with the kinetic data of sodium gathered during the leaching experiment with a slightly higher rate of alteration and equivalent thicknesses compared to all the other elements, as noticed in figure 8b. Consequently, this very small portion of hydrated sodium in the glass, that should form a remaining layer depleted in sodium but could not be detected through SEM is observed by NMR thanks to the high sensitivity of this technique to small nuclei with highly symmetrical sites

like sodium. A significantly higher chemical resistance from one of the crystalline phases would necessarily conduct to a notably different ratio of distribution before and after alteration. In this case, the quantification of the NMR spectra yielded very close ratios translating a relatively low proportion of sodium hydrated. Therefore this result is consistent with a mechanism of alteration mainly driven by hydrolysis that affects similarly the glassy matrix and the crystals with a very slight preferential release of sodium, as expected from a fully vitreous soda-lime glass.

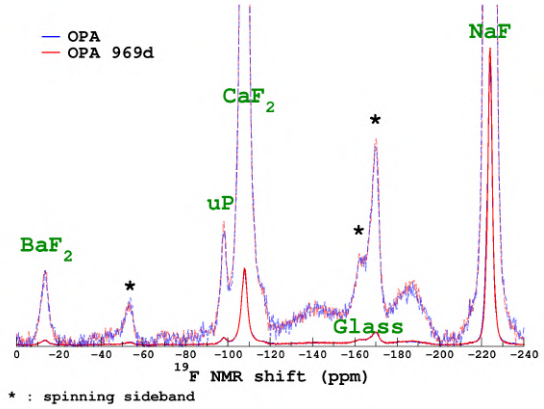

(a) ^{19}F MAS NMR

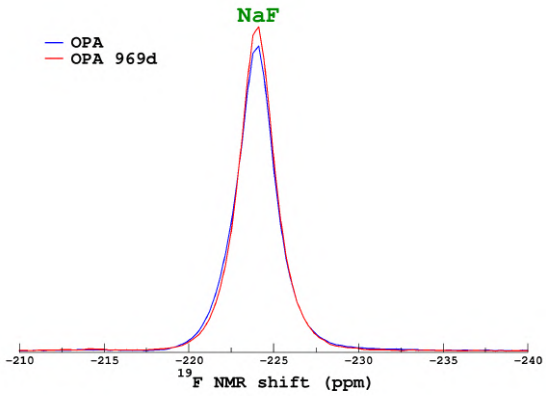

(b) ^{19}F MAS NMR

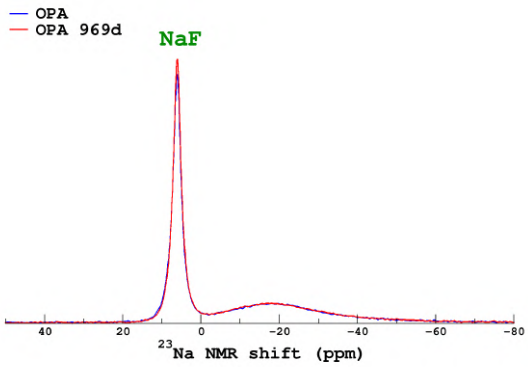

(c) ^{23}Na MAS NMR

FIG. 13: 13a, Experimental MAS NMR ^{19}F spectra obtained from pristine (OPA) and altered for 969 days (OPA 969d) in acetic acid 4 % (v/v) at 70 °C opal crystal glass powder, the dashed lines are amplifications of the spectra shown with solid lines and 13b exhibits a focus on the line of NaF before (OPA) and after alteration (OPA 969d). The same line of NaF seen from ^{23}Na MAS NMR is displayed in figure 13c. All spectra were obtained from the same pristine and altered 969 days opal glass powders at 25 kHz and 11.72 T.

CONCLUSION

Opal crystallized glass plates appear very different at various scales with each scale of analysis bringing up a unique level of information. In the pristine glass we can visually determine at a macroscopic scale a thin vitreous region and an thick opaque region in the width of plate as evidenced by optical microscopy. From a microscopic point of view most of the material is homogeneous except for variations of elements distribution close to the top and bottom surfaces of the plate as explored by low magnification SEM and ToF-SIMS. At a micro to nanometric scale, as observed by TEM with EDS analysis, the glassy matrix is riddled with 3 different types of crystals making it a composite yet compact bulk material. These observations outlined the necessity to study this material from different aspects. Firstly, the bulk material, under the form of powder, used for XRD and NMR analyses which gave us access to high precision data collected on a great number of particles giving an overview of the structure and durability. Structural information regarding the crystalline phases and evidences of fluorine in the glassy matrix were obtained from NMR, when alteration data were collected from the leaching kinetics in solution and the characterization of the remaining altered layer at the surface of the powder was carried out by SEM. As a result seemingly close rates of hydrolysis and interdiffusion were found and no major variations along the 3 years of alteration were noticed from the electronic imaging of altered grains cross-sections. Secondly a slab comprising the top and bottom faces of the plate was altered and characterized through multiple techniques. This slab showed a very different structure with no crystals near the surface and enrichment in Na, Ba and Ca correlated with a depletion in F in the top 10 µm near the top smooth face. After 231 days of alteration, evidences of a higher interdiffusion than hydrolysis rate of alteration were observed from the micron-sized remaining alteration layer analyzed by TEM-EDS, ToF-SIMS and SE. Evidently, the surface and bulk of a single plate do not have the same kinetics nor mechanisms of alteration as the bulk material but overall the great durability of this opal crystallized glass under harsh alteration conditions such as acetic acid 4 % (v/v), at 70 °C for very long periods of time can be outlined. Especially the alteration of the bulk which is governed by the hydrolysis of the material, evolving at a constant, characterized and predictable rate at the same order of magnitude as resistant vitreous silicate glasses reported in the literature Perera and Doremus (1991), Sinton and LaCourse (2001), Stone-Weiss et al. (2020). Regarding the slab, the formation of an alteration layer was observed with potential protective barrier effects of this altered layer that could be studied in itself through an alteration experiment

to gather the kinetics of alteration of the glass slab only.

II. METHODS

A. Glass preparation

Opal glass plates were received directly from the manufacturer. Rectangular glass slabs were cut out from each item and the raw edges were polished to 1 µm (roughness of the order of a few nm), no annealing step was performed. Glass powder with grain diameters ranging from 63 µm to 125 µm was prepared and washed. Then Brunauer-Emmet-Teller (BET) method Brunauer et al. (1938) on a Micromeritics ASAP 2010 instrument with krypton gas was performed on the mentioned powder and the specific surface area of the powder was measured. Finally the ground powders were analyzed by Filab using Inductively Coupled Plasma Atomic Emission Spectroscopy (ICP-AES) to determine the molar composition of the bulk glass which was then normalized and converted to weight percent.

B. NMR spectroscopy

Magic-Angle Spinning Nuclear Magnetic Resonance (MAS NMR) data were collected on a Bruker Avance Neo 500WB spectrometer operating at a magnetic field of 11.72 T. A commercial Bruker CPMAS 2.5 mm (outer diameter of the ZrO_2 rotors) was used at a spinning frequency of 25 kHz. A recycle delay of 32 s and 256 s was used for ^{23}Na and ^{19}F, respectively. The NMR shifts were referenced to external 1 M aqueous NaCl (^{23}Na, 0 ppm), 1.0 M aqueous $Al(NO_3)_3$ (0 ppm) and using the CaF_2 (^{19}F 108 ppm) peak. ^{23}Na and ^{27}Al were acquired using a single sort pulse excitation (1 µsec) whereas, to cancel probe background signal, ^{19}F was acquired using rotor-synchronized Hahn Echo sequence (90–τ–180–τ acquisition, with τ being equal to a single rotor period). Data were processed and fitted using an in-house package (T. Charpentier). For ^{19}F MAS NMR, peaks and spinning sidebands were fitted using a mixture of Gaussian and Lorentzian. For ^{23}Na, NaF peak (centerband and spinning sidebands) were simulated using a single Gaussian lineshapes; the broad glass peak was simply simulated using two Gaussians (to account for the NMR parameter distribution, see Angeli et al. 2010 **?**). In both case (^{19}F and ^{23}Na) the aim of the fit was to quantify each phase contribution.

C. Leaching experiments

Long term alteration in static mode was performed in perfluoroalkoxy alkane reactors (PFA) at 70 ± 3°C in 4 % (v/v) acetic acid solution, which translates to a pH of 2.4 ± 0.1. About 800 mg of 63–125 µm particle size glass powder and a single glass slab were added to a large volume of acetic acid. The precise quantities of solution and glass were carefully measured and the resulting glass-surface-area-to-solution-volume ratio SA/V was calculated. This experiment being designed for long-term alteration, it is likely to use the geometric approximation described in equation 1, rather than the BET measurements. As demonstrated by Fournier et al. Fournier et al. (2016, 2017) BET is very sensitive to nanoscale rugosity which tends to increase the glass surface area significantly and is not so accurate after the first stage of alteration. Both methods of calculation are used in this paper, leading to SA/V initial values of 50.5 m^{-1} using the geometrical approximation given in equation 1 and 92.5 m^{-1} with the classical BET approach. The difference between these 2 values is discussed with the leaching results. Since there was no stirring, the glass powder lied at the bottom of the reactor and the glass slab was elevated by a PFA stand to avoid contact between the slab and the powder.

$$SA_{geo}/V = \frac{3.m_{glass}}{V_{sol}.\rho.R_{mean}} \tag{1}$$

With SA_{geo}/V the glass-surface-area-to-solution-volume-ratio determined with the geometric approximation (m^{-1}), V_{sol} the volume of solution in the experiment (m^3), m_{glass} the mass of glass in the experiment (g), ρ the density of the glass ($g.m^{-3}$) and R_{mean} the mean radius of glass particles in the experiment (m).

The reactor was tightly closed and Teflon ribbon was applied on the screwing neck to make the reactor airtight. Then, the reactor was placed in a secondary reactor, larger and filled with water, to ensure homogeneous temperature and avoid evaporation in the primary reactor.

The alteration solution was regularly sampled from the reactor and the concentrations of glass constituents in solution were analyzed by Inductively coupled Plasma - Atomic Emission Spectroscopy (ICP-AES) after acidification with nitric acid. The solution withdrawal generated by the samplings is considered by recalculating the glass-surface-area-to-solution-volume-ratio after each sampling. The normalized mass loss for each element of each sample was calculated using equation 2.

$$NL_{geo_i} = \frac{C(i)_t}{(SA_{geo}/V)_t . x_i} \tag{2}$$

With NL_{geo_i} the normalized mass loss of element i after t days of alteration ($g.m^{-2}.d^{-1}$), $C(i)_t$ the concentration of element i in solution after t days of alteration ($g.m^{-3}$), SA_{geo}/V_t the glass-surface-area-to-solution-volume-ratio determined with the geometric approximation after t days of alteration (m^{-1}), x_i the mass fraction of element i in the pristine glass

These normalized losses per element can be translated to equivalent thicknesses of glass altered thanks to equation 3 and enable the calculation of alteration rates through partial derivation with respect to time given in equation 4.

$$ETh_{geo_i} = \frac{NL_{geo_i}}{\rho} \tag{3}$$

With ETh_{geo_i} the equivalent thickness of glass altered for element i after t days of alteration (µm), NL_{geo_i} the normalized losses of element i in solution after t days of alteration ($g.m^{-2}.d^{-1}$), ρ the pristine glass density ($g.m^{-3}$).

$$r_i(t) = \frac{\partial NL_{geo_i}}{\partial t} \tag{4}$$

With $r_i(t)$ the releasing rate of an element i for a given time of alteration ($g.m^{-2}.d^{-1}$) and NL_{geo_i} the normalized losses of element i in solution after t days of alteration ($g.m^{-2}.d^{-1}$).

The diffusion coefficients for species with interdiffusion behaviour were calculated using equation 5.

$$D_i = \pi \left(\frac{r_i(t)}{2\rho} \right)^2 \tag{5}$$

With D_i the diffusion coefficient of an element i for a given time of alteration ($m^2.s^{-1}$), $r_i(t)$ the partial derivative of normalized losses of element i with respect to time ($g.m^{-2}.s^{-0.5}$) and ρ the pristine glass density ($g.m^{-3}$).

Correction factors to ensure data consistency throughout the five different campaigns of analysis were computed. For the first and/or last sampling times of an analytical batch, two measurements of the concentration were performed allowing for the calculation of a correction factor f, as broke down in equation 6. This correction factor has then been applied to all the values in the analytical batch using equation 7. This adjustment method was iterated for each analytical batch and the values displayed in the plots of this paper are derived from the adjusted concentrations.

$$f_{corr_j} = \frac{C(i)_{t,j-1} - C(i)_{t,j}}{C(i)_{t,j}} \tag{6}$$

With f_{corr_j} the correction factor, $C(i)_{t,j-1}$ the concentration of element i in solution after t days of alteration obtained from analytical batch $j-1$ (g.m^{-3}), $C(i)_{t,j}$ the concentration of element i in solution after t days of alteration obtained from analytical batch j (g.m^{-3}).

$$C(i)_{corr_t,j} = C(i)_{t,j}.(1 + f_{corr_j}) \tag{7}$$

With $C(i)_{corr_t,j}$ the adjusted concentration of element i in solution from analytical batch j after t days of alteration based on the values obtained from analytical batch $j-1$ (g.m^{-3}), $C(i)_{t,j-1}$ the concentration of element i in solution after t days of alteration obtained from analytical batch $j-1$ (g.m^{-3}), $C(i)_{t,j}$ the concentration of element i in solution after t days of alteration obtained from analytical batch j (g.m^{-3}).

After 231 days of alteration the glass slab was removed from the reactors, washed with deionized water and slowly dried to be characterized by Tof-SIMS and spectroscopic ellipsometry. The powder, which was responsible for more than 97 % of elemental release in solution, remained in the reactor and samplings were carried on until 1096 days, which corresponds to exactly 3 years of alteration.

D. ToF-SIMS

Depth profiles were analyzed on the smooth face of the pristine and altered glass slabs by Time of Flight Secondary Ion Mass Spectroscopy (ToF-SIMS) with an IONTOF TOF 5 instrument at

Tescan Analytics (France) using O^{2+} sputtering and Bi^{+} analyzing beams scanning a surface area of 50 × 50 µm^2. Oxygen beam was tuned at 1 keV and 130 nA and only positive mode was used excluding the analysis of fluorine. The depth of the craters was measured after the analyses, and profiles were calculated assuming that the sputtering rate was constant. First of all, at each mass analysis, the intensity of each element was individually normalized to the total intensity accounting for all the ions collected to rectify any fluctuation from the ion source, as shown in equation 8. Then, the profiles of interest were normalized to the mean value obtained in the pristine glass with equation 9 to cut off the signal of the pristine glass and evaluate the relative behavior of each element in the altered glass. All elements are thus normalized to 1 in the pristine glass. Finally, the data have been normalized compared to pristine glass and Si using equation 10, since the leaching rate of Si was the lowest and thus considered as the least mobile element in this glass after 231 days of alteration.

$$J_i = \frac{A_i}{A_{tot}} \tag{8}$$

With J_i the intensity of element i normalized to the total count of ions, A_i the intensity of element i and A_{tot} the total intensity collected on the mass spectrometer.

$$J_{norm_i} = \frac{J_i}{\frac{1}{n_{sup} - n_{inf}} \sum_{n_{inf}}^{n_{sup}} J_i} \tag{9}$$

With J_{norm_i} the intensity of element i normalized to the pristine glass, J_i the intensity of element i normalized to the total count of ions, n_{inf} corresponding to a point in the pristine glass, n_{sup} corresponding to the maximum profile depth.

$$J_{norm_{Si_i}} = \frac{\frac{J_i}{J_{Si}}}{\frac{1}{n_{sup} - n_{inf}} \sum_{n_{inf}}^{n_{sup}} \frac{J_i}{J_{Si}}} \tag{10}$$

With $J_{norm_{Si_i}}$ the intensity of element i normalized to the pristine glass and Si, J_i the intensity of element i normalized to the total count of ions, J_{Si} the intensity of Si normalized to the total count of ions, n_{inf} corresponding to a point in the pristine glass, n_{sup} corresponding to the maximum profile depth.

For initial glass constituting elements (i.e. Si, Al, Na, Ba, Ca), the thickness of glass depleted for each element has been estimated by collecting the depth corresponding their maximal normalized intensity J_{norm_i}. The hydrated depth of the sample has been determined by considering the depth of H^+ and $SiOH^+$ species when the normalized intensity J_{norm} reaches 1. Please note that the ionic form exhibited in the figure's legend or in the text do not represent the ionization of the elements in the glass sample but the species detected by the seconary ion mass spectrometer after sputtering.

E. Spectroscopic Ellipsometry

The glass slab altered 231 days has been roughen with SiC grinding paper on one large side to prevent the back-side reflection during the ellipsometry measurements. The sample was then thoroughly cleaned, and the analysis was carried out at the Pennsylvania State University in the Department of Chemical Engineering and Materials Research Institute. Detailed procedures and explanations are available in Ngo et al. Ngo et al. (2018). In ellipsometry, information about the sample under the study is obtained by fitting measured ellipsometric spectra to an optical model. The current study used a rotating compensator spectroscopic ellipsometer (J.A. Woollam Co. Alpha-SE) that had a wavelength range of 381 - 893 nm. The incident angle of light used in the study was 70°. The measurements were carried out at room relative humidity (40-50 %). Pristine glass slab was first measured and analyzed, and the obtained optical properties were used as the substrate in the optical model of the altered sample. The SE spectra fittings in this study were performed using the CompleteEASE software package. The optical model for the altered glass sample included multiple sub-layers for the alteration layer on top of the substrate (pristine glass). Each sub-layer consisted of a glass and a void (porosity) component, and the Bruggeman effective medium approximation (EMA) was used in calculating the optical response of each sub-layer in the alteration layer (Aspnes et al. (1979)). In the SE analysis, each sub-layer was assumed to be optically isotropic and the boundaries between them to be parallel. The pore sizes were considered to be small in comparison to the wavelength of the incident light. This assumption was required to validate the use of the EMA. It was also assumed that the optical properties of the solid part of the leached layer are the same as those of the studied pristine glass. This assumption was made due to the difficulty in accurately determining the refractive index of the solid part and the fraction of porosity of each sub-layer in the alteration layer.

F. Scanning electron microscopy

The morphology of the pristine slab and powder and the altered powder were examined by field emission gun-scanning electron microscopy (FEG-SEM) using a Zeiss Supra 55 at 15 kV (probe current about 1 nA). To allow precise mapping the samples were embedded in an epoxy resin and polished before coating with a 15 nm carbon layer for electronic conduction. The determination of the chemical distribution of the different phases within the samples was obtained from energy dispersive X-ray spectroscopy (EDS) analyses on plane polished samples with a Bruker AXS X-FlashDetector 4010 system. Data collection and treatment were done with the ESPRIT2.0 software (Bruker^{TM}, USA)

G. X-Ray Diffraction

X-Ray diffraction patterns were collected on a D8 advance diffractometer from Bruker operating at 35 kV and 40 mA, using Co-Kα radiation (1.79 Å) at an angular step of 0.01 degree per second between 3.0 and 80.0 degrees (2θ) angles. The EVA software coupled with the ICDD pdf-2 database enabled the identification of the major phases in the materials. Prior to XRD experiments, opal glass samples were crushed and ground in a tungsten ball mill and sifted in a 32 µm sieve. After sieving, samples powders were sprinkled gently in XRD sample holder using a 65 µm sieve. The top layer was removed carefully by cutting the surface with a thin razor blade leading a smooth surface without compaction: such preparation allows to decrease the preferential orientation of particles.

H. Transmission Electron Microscopy coupled with Energy Dispersive X-Ray Spectrometry

Nanoscale characterization was performed by transmission electron microscopy on ultrathin sections. Samples were prepared by focused ion beam milling with an FEI FIB 200 SEM system or with a FEI Hélios NanoLab 650 Dual beam microscope. During FIB preparation, a few nanometers thick layer of carbon was first applied on the samples to make them conductive. Then two few micrometers thick layers of platinum (Pt) and palladium (Pd) were then coated on the surface to protect the samples. Afterwards the FIB cuts were carved and thinned using gallium (Ga) ions beam. TEM observations were carried out on a FEI Tecnai F20 microscope equipped with a field emission gun, a GATAN scanning device (STEM) and a complete set of

detectors that allows image acquisition in a range of operating modes (dark field, bright field, high angle annular dark field) and a spatial resolution of 0.24 nm. The STEM is coupled with a Si(Li) detector (EDAX Sapphire r-TEM): the Energy Dispersive X-ray spectrometry capability coupled to the TIA ES Vision software (FEI inc.) were used to determine the chemical composition of the compounds and phases of interest. During TEM observations and analyses, we had to face and solve two problems: *i)* the FIB preparation by ions milling required protection layers and generated implementation of elements inside the studied materials: in all observations we had to consider the implementation of Ga for example and slight diffusion of platinum at the extreme surface of the samples; *ii)* the opal glasses studied in this work turned out to react strongly under the electron beam: to limit the irradiation damage and to make the analyzes more reliable, sometimes requiring long acquisition times, we sometimes had to limit the accelerating voltage of the electrons in order to limit their energy, and an observation and analysis protocol adapted to each sample had to be implemented in order to obtain reliable information and quality data on the opal glasses studied.

DATA AVAILABILITY

The data that supports the findings of this study are available from the corresponding author upon reasonable request.

ACKNOWLEDGEMENTS

This study was supported by the French Agency for Research (ANR, PRCE program, grant 18-CE08-0025). Prime Verre prepared the glass slabs and glass powders. Elodie Chauvet, Loan Lai, Florian Cousy and Yves Depuydt from Tescan analytics performed the Tof-SIMS profiles. Géraldine Parisot analyzed the solutions by ICP-AES. Filab analyzed the glass composition. Patrick Jollivet is acknowledged for igniting this experimental work. Myriam Duc from the GERS department of Université Gustave Eiffel is acknowledged for her invaluable help and assistance for the X-Ray Diffraction experiments. Laurent Gautron would like to particularly thank Eric Leroy (ICMPE, Université Paris-Est Créteil) for his assistance, his skills and always in a good mood during the observations and analyzes by transmission electron microscopy.

AUTHOR CONTRIBUTION

PA and LB performed the leaching experiments, LB carried out the MO and SEM observations and all the data curation. LG was responsible for the TEM preparations and observations. TC performed the NMR studies. HK and SHK took care of the spectroscopic ellipsometry. FA, SG and LB supervized the study and worked on the conceptualization, methodology and original draft. All the authors helped on the paper editing.

COMPETING INTERESTS

The authors declare no competing interests.

Hélène Aréna, Diane Rébiscoul, Emmanuelle Garcès, and Nicole Godon. Comparative effect of alkaline elements and calcium on alteration of International Simple Glass. *npj Materials Degradation*, 3(1):10, December 2019. ISSN 2397-2106. doi:10.1038/s41529-019-0072-7. URL http://www.nature.com/articles/s41529-019-0072-7.

D. E. Aspnes, J. B. Theeten, and F. Hottier. Investigation of effective-medium models of microscopic surface roughness by spectroscopic ellipsometry. *Physical Review B*, 20(8):3292–3302, October 1979. doi: 10.1103/PhysRevB.20.3292. URL https://link.aps.org/doi/10.1103/PhysRevB.20.3292.

Stephen Brunauer, P. H. Emmett, and Edward Teller. Adsorption of Gases in Multimolecular Layers. *Journal of the American Chemical Society*, 60(2):309–319, February 1938. ISSN 0002-7863, 1520-5126. doi:10.1021/ja01269a023. URL https://pubs.acs.org/doi/abs/10.1021/ja01269a023.

B.C. Bunker. Molecular mechanisms for corrosion of silica and silicate glasses. *Journal of Non-Crystalline Solids*, 179:300–308, November 1994. ISSN 00223093. doi:10.1016/0022-3093(94)90708-0. URL https://linkinghub.elsevier.com/retrieve/pii/0022309394907080.

1986 Ceramic cookware in contact with food — Release of lead and cadmium —. ISO 8391-1:1986.

Marie Helene Chopinet, M. Verità, R. Falcone, P. Lehuédé, M. Vallotto, Michele Nardone, and A. Sodo. Soda-Lime-Silica Glass Containers: Chemical Durability and Weathering Products. In *Glass – The Challenge for the 21st Century*, volume 39 of *Advanced Materials Research*, pages 305–310. Trans Tech Publications Ltd, 2008. doi:10.4028/www.scientific.net/AMR.39-40.305.

Marie Collin, Maxime Fournier, Thibault Charpentier, Mélanie Moskura, and Stéphane Gin. Impact of alkali on the passivation of silicate glass. *npj Materials Degradation*, 2(1):16, December 2018. ISSN 2397-2106. doi:10.1038/s41529-018-0036-3. URL http://www.nature.com/articles/s41529-018-0036-3.

G Engelhardt and D Michel. High-resolution solid-state NMR of silicates and zeolites. January 1987. URL https://www.osti.gov/biblio/6743230.

Maxime Fournier, Aurélien Ull, Elodie Nicoleau, Yaohiro Inagaki, Michaël Odorico, Pierre Frugier, and Stéphane Gin. Glass dissolution rate measurement and calculation revisited. *Journal of Nuclear Materials*, 476:140–154, August 2016. ISSN 00223115. doi:10.1016/j.jnucmat.2016.04.028. URL https://linkinghub.elsevier.com/retrieve/pii/S0022311516301386.

Maxime Fournier, Michaël Odorico, Elodie Nicoleau, Aurélien Ull, Pierre Frugier, and Stéphane Gin. Reactive Surface of Glass Particles Under Aqueous Corrosion. *Procedia Earth and Planetary Science*, 17:257–260, 2017. ISSN 18785220. doi:10.1016/j.proeps.2016.12.049. URL https://linkinghub.elsevier.com/retrieve/pii/S1878522016300819.

Dieter Freude and Jürgen Haase. Excitation of Quadrupolar Nuclei in Solids. In *Quadrupole Effects in Solid-state NMR, Basic Principles and Experimental Techniques for Nuclei with Half-integer Spins*. Leipzig, 2019.

Odile Majérus, Patrice Lehuédé, Isabelle Biron, Fanny Alloteau, Sathya Narayanasamy, and Daniel Caurant. Glass alteration in atmospheric conditions: crossing perspectives from cultural heritage, glass industry, and nuclear waste management. *npj Materials Degradation*, 4(1):27, December 2020. ISSN 2397-2106. doi:10.1038/s41529-020-00130-9. URL http://www.nature.com/articles/s41529-020-00130-9.

Dien Ngo, Hongshen Liu, Nisha Sheth, Raymond Lopez-Hallman, Nikolas J. Podraza, Marie Collin, Stéphane Gin, and Seong H. Kim. Spectroscopic ellipsometry study of thickness and porosity of the alteration layer formed on international simple glass surface in aqueous corrosion conditions. *npj Materials Degradation*, 2(1):20, December 2018. ISSN 2397-2106. doi:10.1038/s41529-018-0040-7. URL http://www.nature.com/articles/s41529-018-0040-7.

Gunarathna Perera and Robert H. Doremus. Dissolution Rates of Commercial Soda-Lime and Pyrex Borosilicate Glasses: Influence of Solution pH. *Journal of the American Ceramic Society*, 74(7):1554–1558, July 1991. ISSN 0002-7820, 1551-2916. doi:10.1111/j.1151-2916.1991.tb07139.x. URL http://doi.wiley.com/10.1111/j.1151-2916.1991.tb07139.x.

Sandra Rio, Christine Andraud, Philippe Deniard, Catherine Dacquin, Rodolphe Delaval, Sébastien Donze, and Stéphane Jobic. Study of the influence of crystalline phases on optical characteristics of a glass-ceramic in the visible range via simulations by the four-flux method. *Journal of Non-Crystalline Solids*, 551:120446, January 2021. ISSN 00223093. doi:10.1016/j.jnoncrysol.2020.120446. URL https://linkinghub.elsevier.com/retrieve/pii/S0022309320305573.

Christopher W. Sinton and William C. LaCourse. Experimental survey of the chemical durability of commercial soda-lime-silicate glasses. *Materials Research Bulletin*, 36(13-14):2471–2479, November 2001. ISSN 00255408. doi:10.1016/S0025-5408(01)00724-3. URL https://linkinghub.elsevier.com/retrieve/pii/S0025540801007243.

Nicholas Stone-Weiss, Randall E. Youngman, Ryan Thorpe, Nicholas J. Smith, Eric M. Pierce, and Ashutosh Goel. An insight into the corrosion of alkali aluminoborosilicate glasses in acidic environments. *Physical Chemistry Chemical Physics*, 22(4):1881–1896, 2020. ISSN 1463-9076, 1463-9084. doi:10.1039/C9CP06064B. URL http://xlink.rsc.org/?DOI=C9CP06064B.

Appendix A: Supplementary information

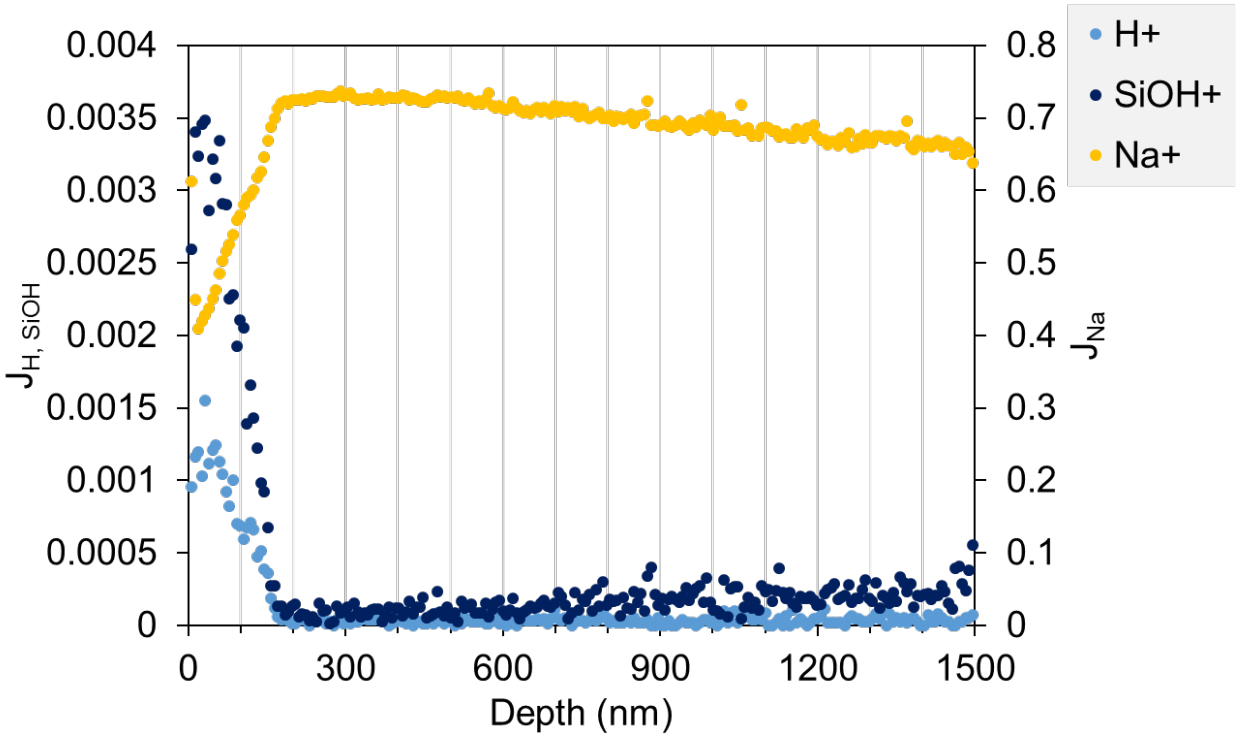

FIG. 14: ToF SIMS profiles obtained from the analysis of the smooth face of a pristine opal crystallized glass plate. The ions displayed represent the species detected by the Mass spectrometer after sputtering. The signals are normalized to the total intensity. Signals from H and SiOH are read on the left hand Y-axis and signal from Na is read on the right hand Y-axis.

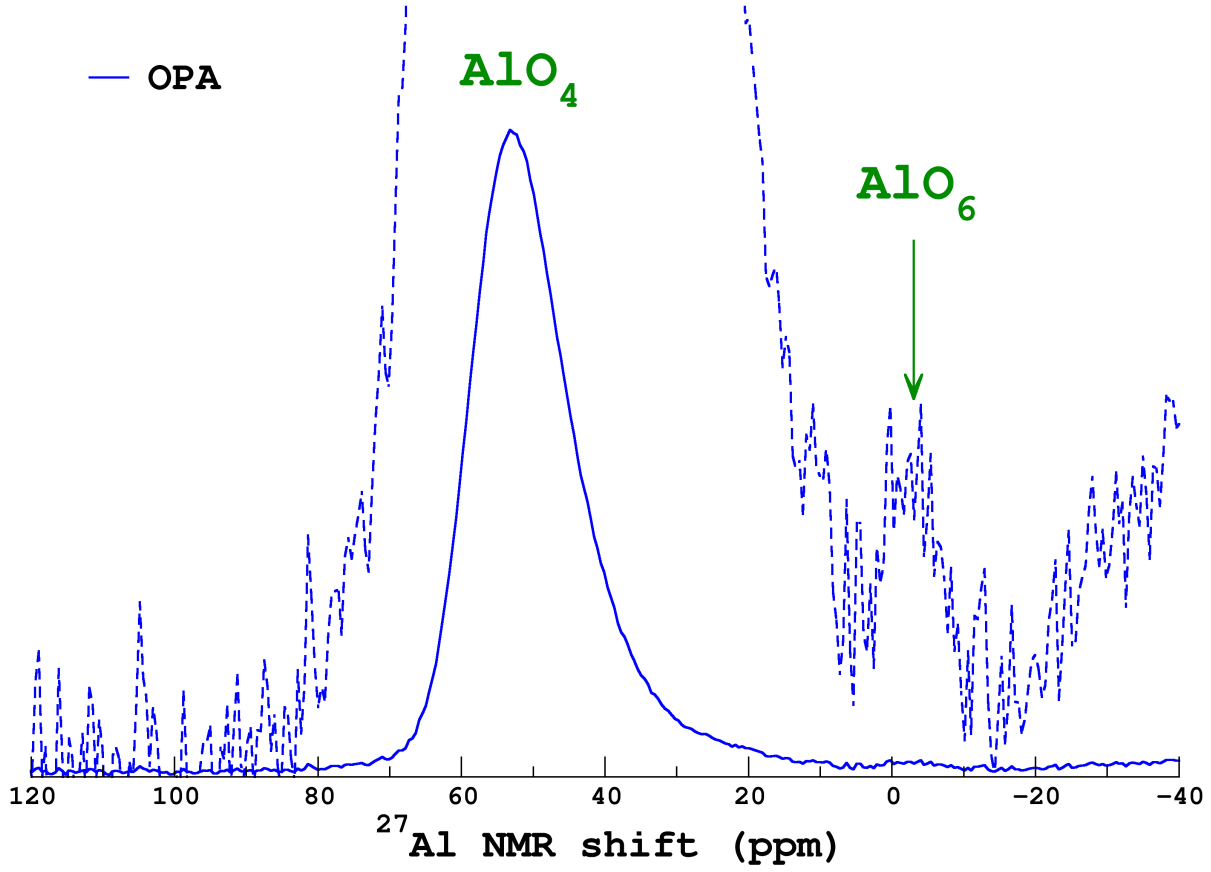

FIG. 15: Experimental MAS NMR ^{27}Al spectrum obtained from pristine opal glass powder at 11.72 T and 25 kHz. The dashed line is an amplification of the solid line spectrum.

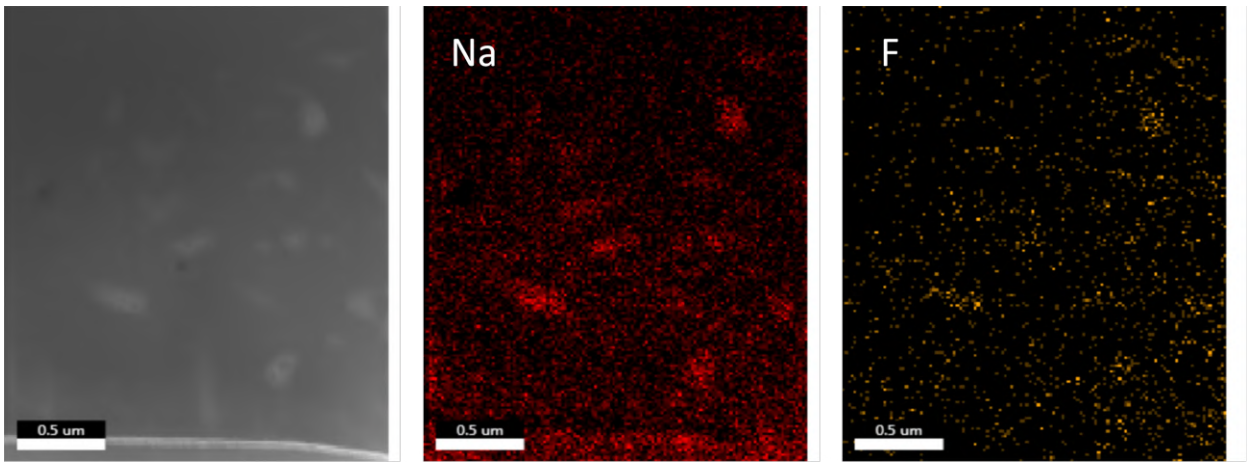

FIG. 16: Back-Scattered Electron TEM image of a selected area in the opal glass slab (left); EDS mappings of sodium Na (middle) and fluor F (right) from the same region.

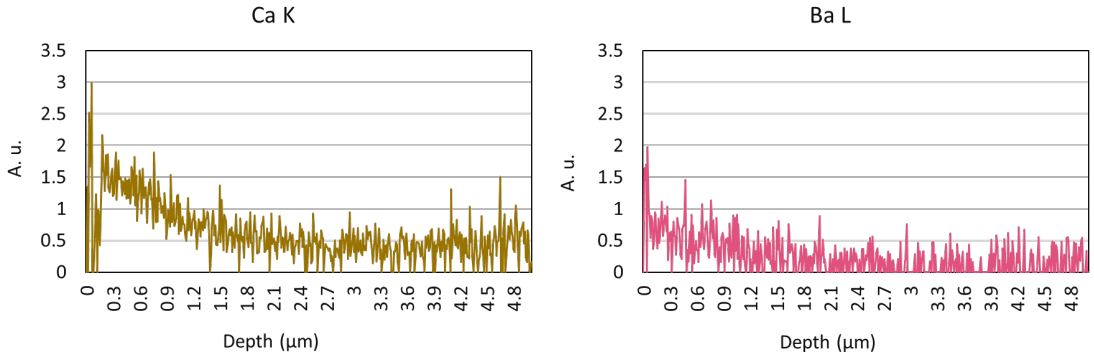

(a) Ca TEM-EDS

(b) Ba TEM-EDS

FIG. 17: 17a EDS-TEM profile for calcium (K-spectral line) in a selected area of the 231-days-altered opal glass. 17b EDS-TEM profile for barium (L-spectral line) in a selected area of the 231-days-altered opal glass. The high peaks just below the surface are probably due to the presence of the Pt-Pd protection layers which are expected to favor the migration of elements like Ca and Ba.

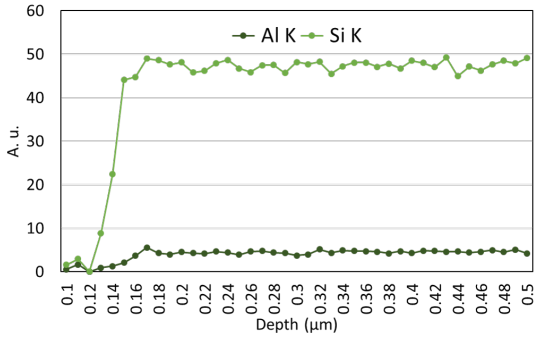

FIG. 18: EDS-TEM profile for aluminum (K-spectral line) and silicon (K-spectral line) in a selected area of the 231-days-altered opal glass.